PRECISION LARGE-AREA LOW TEMPERATURE BLACKBODY BB-100V1 FOR IR CALIBRATIONS

CONCEPTUAL DESIGN AND COMPUTER MODELING

VIRIAL, INC.

Gaithersburg, MD
February 2005

Contents

1. Objectives of Work and Design Targets 3
2. General Background and Design Concepts Developing 4
   2.1. Black coating selection 4
   2.2. Selection of Method for Cavity Thermal Stabilization 5
3. Choice of Cavity Shape and Preliminary Assessment of Effective Emissivity 6
   3.1. Definitions of Principal Quantities 6
   3.2. Method and Software for Effective Emissivity Modeling 7
   3.3. Background radiation effect 8
   3.4. Selection of Cavity Geometry 9
   3.5. Results of Monte Carlo Calculations for Isothermal Cavity 10
4. Steady-State Temperature Distribution FEA Analysis 11
   4.1. Statement of a Problem 11
   4.2. Radiation Losses from Cavity Internal Surface 12
   4.3. Thermophysical Modeling using ANSYS 8.0 13
5. Evaluation of Thermal Inertia Constant 19
6. Monte Carlo Modeling of BB-100V1 Effective Emissivity 21
7. BB-100V1 Preliminary Design 23
8. References 24

1. Objectives of Work and Design Targets

The major design requirements and targets are shown below in the Table 1.

Table 1. BB100-V1 Design Targets

Parameter	Required Value
Maximum operating temperature	350 K (77ºC)
Minimum operating temperature	240 K (-33ºC)
Spectral range	1.5 μm – 15 μm
Cavity effective emissivity	0.99
Opening (non-precision aperture)	Ø100 mm
System Field-of-View (FOV)	12 mrad (0.688º)
Environment operation conditions	Vacuum chamber (10^{-6} Torr, below 100 K)
	Air environment (clean room at 23 ± 3ºC)
Temperature non-uniformity across opening	0.1 K
Temperature set point resolution	0.01 K
Maximum temperature instability under thermostabilization	0.05 K
Limitation on the blackbody warning-up time (approx.)	2 hrs.
Total Wattage (approx.)	2500 W
Input Voltage	100 V AC or 200 V AC
Blackbody temperature set up and control	External controller with RS-232 interface to (optional) PC computer
Temperature sensor for control system	Pt RTD
Thermometers of blackbody	5 pieces
Calibration traceability of Pt RTD to NIST	Yes. Calibration traceability to NIST is assumed for 1 (one) Pt RTD only
Operating Environment Pressure	10^{-6} Torr
Orientation of the blackbody	Facing down (±30º leaned)
Cable length	5 m for inside vacuum chamber and 5 m for outside chamber

2. General Background and Design Concepts Developing

2.1. Black coating selection

While identifying appropriate coating for BB-100V1 bottom, we were looking for black materials or paints possessing emissivity better 0.9 in the spectral range of interest, as well as low outgassing properties. There are several comprehensive reviews [1-6] on application and optical properties of black paints and various coatings to stray light suppressing, solar energy absorbing, for thermal detectors of optical radiation, radiation losses control, etc. After comparative analysis of literature data, the Nextel (former 3M) Velvet Coating 811-21 was chosen.

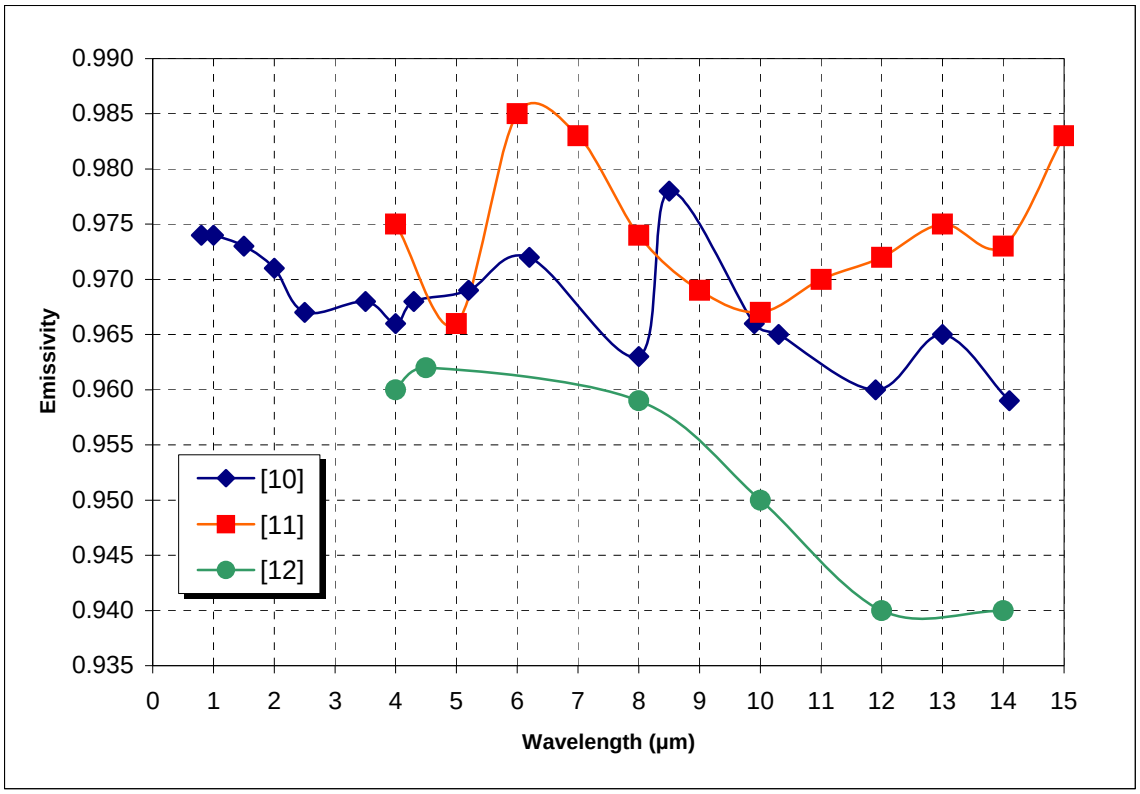

Fig. 1. Spectral emissivity of Nextel Velvet Coating 811-21 according to [10-12].

This black coating uses extensively in infrared radiometry during more than 25 years [7-12]; it can be exploit in cryo-vacuum environment. Moreover, Vega International has a broad experience of its use in a variety of radiometric systems developed. The data on spectral emissivity of Nextel 811-21 extracted from [10-12] are depicted in Fig. 1.

The curve obtained by PTB (Germany) [11] is the spectral normal emissivity; another curve obtained by BNM/LNE (France) [12] is the spectral directional emissivity for the angle of 12º with the normal. Only the curve [10] spans the entire spectral range of interest. The spectral dependences shown in Fig. 1 are obtained under different measurement conditions; the coatings are laid on various substrates. Furthermore, the optical properties of paint depend substantially upon individual style of its application. For our purposes, it is enough to assume that the spectral hemispherical emissivity of Nextel 811-21 is within 0.935…0.990 interval for wavelength range from 1.5 to 15 μm. The measurements of reflectance performed for the predecessor of Nextel 811-21, the 3M Velvet Black [4], show the presence of a small specular component, less than 10% from overall hemispherical reflectance; the diffuse component of reflectance has the near-Lambertian BRDF [6].

Nextel® Velvet Coating 811-21 can be purchased from Mankiewicz Gebr. & Co [13]; the recommendations of its application can be found at www.upcoat.com. It is recommended to use Nextel® Primer 5523 as a ground and Nextel® 8061 as a solvent. After filtration using the 500/850 filter, the coating should be air-sprayed under pressure of 3.0-4.0 Bar through the spray-nozzle of 1.5 – 1.8 mm in diameter. The drying time is 15-20 min. Outgassing can be performed ambient temperature for 24 hrs, or, at elevated temperature, after 15-40 min of withering in area. The outgassing time in a furnace is 60 min at 80ºC; 30 min at 120ºC.

2.2. Selection of Method for Cavity Thermal Stabilization

The following main methods are used to attain the temperature uniformity of radiating cavities:

1. Radial heat pipe as a structure with very high effective thermal conductivity can be used for thermal stabilization of a radiating cavity [14, 15]. However, it is difficult to span entire temperature range under consideration (240 K to 350 K, or about –33ºC to +77ºC) by one heat pipe with a particular heat transfer agent. So, ammonia heat pipe works effectively only within –60ºC to +50ºC temperature range; water heat pipe – from 50ºC to 270ºC.
2. Implicit resistive heating. This simplest method employs electric heating elements to ensure isothermality of a cavity (see, for instance, [22, 23]). To compensate variable heat losses from internal surface of a cavity, one can applied non-uniform

arrangement of heater, or non-uniform input of electric power to separate heating elements.

3. Immersing the cavity radiator into liquid bath [16-19]. This method is unfitted to vacuum environment.
4. Thermal stabilization of a cavity by a liquid agent fed from an external thermostat [20,21].

As it was agreed with the customer, the last method of thermal control and stabilization has been approved for BB100-V1.

3. Choice of Cavity Shape and Preliminary Assessment of Effective Emissivity

3.1. Definitions of Principal Quantities

The directional spectral effective emissivity of a non-isothermal cavity is a function of the selected reference temperature T_0 and is defined as

$$\varepsilon_e(\xi,\omega,\lambda,T_\xi,T_{ref}) = \frac{L_{\lambda e}(\xi,\omega,\lambda,T_\xi)}{L_\lambda^{bb}(\lambda,T_{ref})}, \quad (1)$$

where $L_{\lambda e}(\xi,\omega,\lambda,T_\xi)$ is the spectral radiance of the effective (i.e. the sum of emitted and reflected) radiation of an infinitesimal element of the cavity wall with coordinate ξ and temperature T_ξ in direction ω at wavelength λ; $L_\lambda^{bb}\left(\lambda,T_{ref}\right)$ is the spectral radiance of a perfect blackbody determined by Planck's law.

An important special case of the local directional effective emissivity is the local normal effective emissivity $\varepsilon_{e,n}\left(r,\lambda,T_{ref}\right)$. It corresponds to viewing the aperture of an axisymmetric cavity along an infinitely thin ray passing parallel to the cavity axis and crossing the aperture plane in the point with radial coordinate *r*.

The average normal effective emissivity $\varepsilon_{e,n}$, which is used in typical calibration arrangements, can be considered as an averaging on cavity aperture:

$$\varepsilon_{e,n}(\lambda, T_{ref}) = \frac{2}{R_a} \int_0^{R_a} \varepsilon_{e,n}(r, \lambda, T_{ref}) r dr \,, \qquad (2)$$

where R_a is the radius of cavity aperture.

By analogy, the average directional and conical effective emissivities can be introduced (see. Fig. 2).

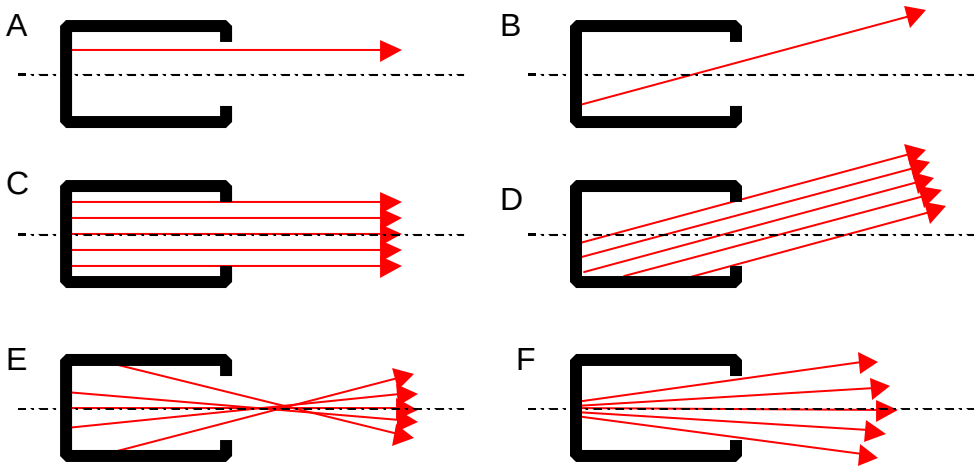

Fig. 2. Various types of effective emissivity (EE): A – local normal EE; B – local directional EE; C – average normal EE; D – average directional EE; E, F – conical EEs.

3.2. Method and Software for Effective Emissivity Modeling

The computation of effective emissivity for blackbody under development was performed by means of STEEP3 [24] modeling software, based on the Monte Carlo algorithm [25-28] that briefly depicted below.

The analysis is restricted to the case of the uniform specular-diffuse reflection model that assumes:

(i) The surface emits diffusely (according to Lambert's law), with an emissivity ε.

(ii) The hemispherical reflectance $\rho = 1 - \varepsilon$ does not depend on incidence angle and is a sum of two components – specular ρ_s and diffuse ρ_d.

(iii) The surface diffusity defined as $D = \rho_d/\rho$ does not depend on incidence angle.

Moreover, the validity of ray optics approximation is assumed, diffraction effects are considered as negligible, and radiation is entirely depolarized due to multiple reflections.

The Monte Carlo method of the radiation transfer simulation is based on a ray-tracing algorithm. For the calculation of the effective emissivity of the cavity by the Monte Carlo method the radiative flux is represented by a large number of rays moving along rectilinear trajectories. The radiation heat transfer inside the cavity is simulated by a random Markov's chain of reflections of these rays with the internal cavity surface. To reduce the dispersion of calculation and decrease the computing time, the method of statistical weights was used.

For the calculation of the effective emissivity, the optical reciprocity theorem and the technique of inverse ray tracing were used. The rays with a statistical weight of unity were directed from a point of observation towards the opening of cavity, and their history was followed until they escape from the cavity or until their statistical weight became less than the given truncation value δ. The last point of reflection is considered as the point of birth of the ray propagating in the inverse direction.

Spectral radiance along the ray exiting from the cavity opening is proportional to

$$\varepsilon_1 P(\lambda,T)+\rho_1(\varepsilon_2 P(\lambda,T_k)+\rho_2(\varepsilon_3 P(\lambda,T_k)+\rho_3(\varepsilon_4 P(\lambda,T_k)+...)...) \qquad (3)$$

where ε_k, ρ_k and T_k are the spectral emissivity, spectral reflectance and temperature of the cavity wall at the point of k-th reflection, respectively; $P(\lambda,T)$ is Planck's function.

After choosing the reference temperature T_{ref}, it is possible to evaluate the effective emissivity of the cavity by following the histories of a large number of rays n, the direction of which are chosen randomly following the given conditions of observation:

$$\varepsilon_e(\lambda,T_{ref}) = \frac{1}{nP(\lambda,T_{ref})}\sum_{i=1}^{n}\sum_{j=1}^{m_i}\varepsilon_j P(\lambda,T_j)\prod_{k=1}^{j-1}\rho_k, \qquad (4)$$

where m_i is the number of reflections in i-th ray trajectory.

We were assumed $\delta = 10^{-5}$ and $N = 10^6$, what it is ensured the uncertainty of effective emissivity calculation $\Delta\varepsilon_e \approx 0.0001$.

3.3. Background radiation effect

The approximation of isothermal cavity implies non-radiating environment. Real ambience has the temperature greater than absolute zero, therefore, must emit thermal radiation that irradiates the aperture of a cavity, and can reach the detector after multiple reflections inside a cavity. Because the spectral, spatial, and angular distributions of background radiation are hard to predict, the simplest case of isotropic blackbody radiation that corresponds to an environmental temperature T_e is usually considered. It is assumed that it is possible to neglect the radiation exchange between cavity and detector,

and detector does not distort the isotropy of background radiation. Let us suppose that the cavity is isothermal at a reference temperature T_{ref} and has effective emissivity ε_e determined for a case of non-radiating background and any geometry of cavity radiation collecting. The effect of isotropic background at temperature T_e can be computed by the equation

$$\varepsilon'_e\left(\lambda, T_{ref}\right) = \varepsilon_e + \left(1-\varepsilon_e\right)\frac{\exp\left(\dfrac{C_2}{\lambda T_{ref}}\right)-1}{\exp\left(\dfrac{C_2}{\lambda T_e}\right)-1}, \qquad (5)$$

for spectral effective emissivity. Here $C_2 = 1.43877\cdot10^{-2}$ m·K is the second radiation constant in Planck's law.

Note that spectral effective emissivity becomes wavelength-dependent even for isothermal cavity with gray internal surfaces as soon as the temperatures of a cavity and an environment are different. The addends in Eqs. (5) (a correction terms for background radiation) vanish when $T_e \to 0$. For nonisothermal cavity, due to additivity of radiant fluxes, the expressions for correction terms on background radiation remain the same – we only must know the effective emissivity of an appropriate isothermal cavity determined for non-emitting environment.

3.4. Selection of Cavity Geometry

We have selected a cylindrical shape of a cavity because for this shape, the selected method of thermostabilization implements simply by wrapping the tube with liquid agent around the cylindrical surface. Due to relatively small FOV (0.012 mrad), the radius R of a cavity shouldn't be significant greater than the aperture radius R_a = 50 mm. We have chosen R = 60 mm and cavity depth L = 200 mm.

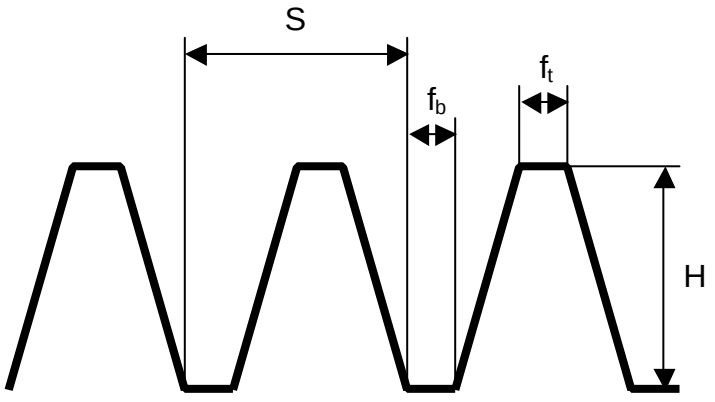

Fig. 3. Geometry of concentric grooves on the bottom of a cavity.

It is known that the normal effective emissivity of a cylindrical cavity with a flat bottom is sharply decreasing if the surface of a bottom has a specular component of reflection. To avoid this effect, we use concentric grooves on cavity bottom. We considered the grooves of a trapezoidal profile as depicted in Fig. 3: $S = H = 5$ mm; $f_b = f_t = 0.2$ mm.

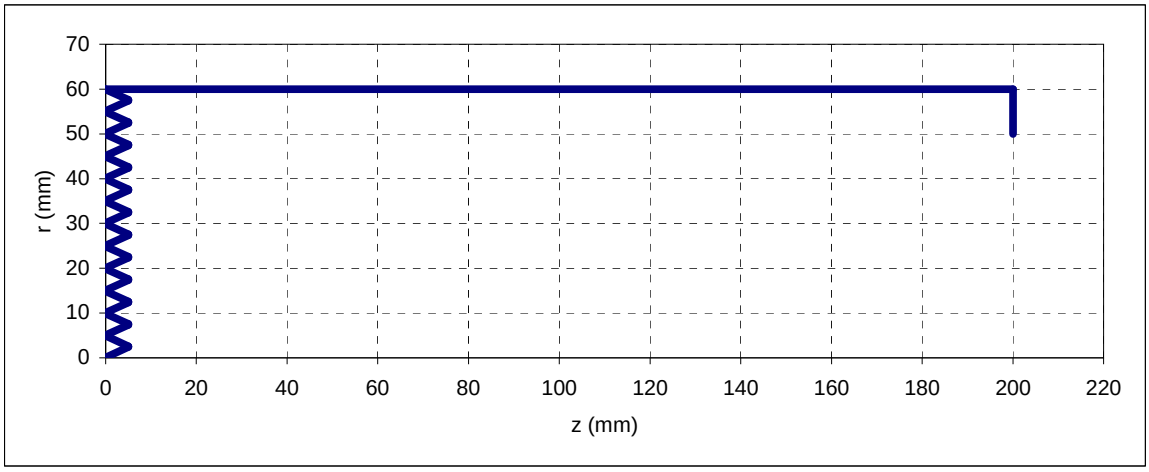

Fig. 4. Cavity generatrix.

The overall scheme of cavity generatrix is depicted in Fig. 5. For the given FOV, the only bottom (excluding its narrow peripheral annulus) is viewable.

3.5. Results of Monte Carlo Calculations for Isothermal Cavity

We have performed the computations of the normal effective emissivities of an isothermal cavity depicted in Fig. 4 using STEPP3 software. We have used the limiting values of wall emissivity (0.935 and 0.990) and 4 values of wall diffusity. The results of computations are presented in Table 2.

Table 2. Normal Effective Emissivity of an Isothermal Cavity

Cavity Wall Emissivity	Cavity Wall Diffusity			
	0.7	0.8	0.9	1.0
0.935	0.9972	0.9976	0.9980	0.9983
0.990	0.9996	0.9996	0.9997	0.9997

4. Steady-State Temperature Distribution FEA Analysis

4.1. Statement of a Problem

It is necessary to evaluate the temperature distribution over internal surface of a cavity. It is significantly depends upon design features that determine all heat sources and sinks. We have built the simplified thermophysical model of BB100-V1 as it is shown in Fig. 5.

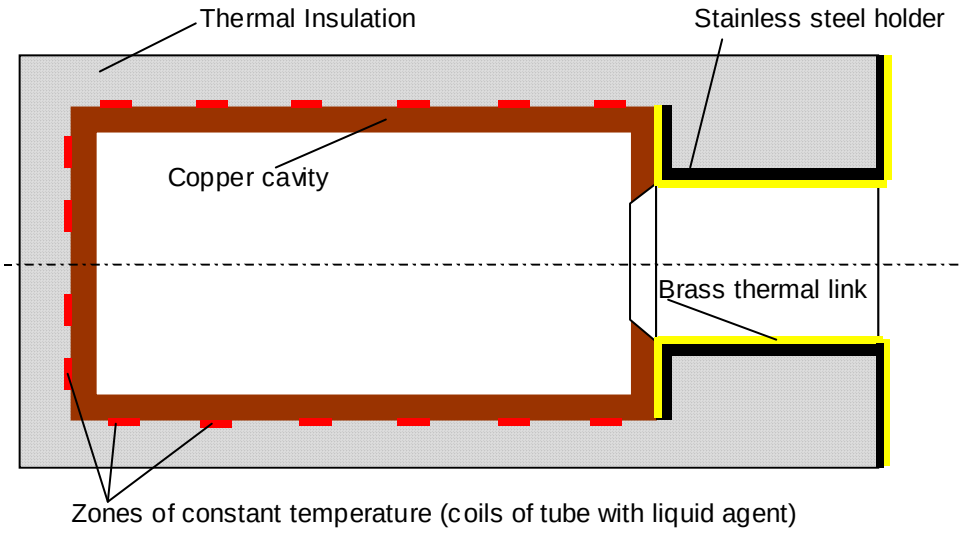

Fig. 5. The simplified thermophysical model of BB100-V1.

We have assumed that the temperatures of the edge of stainless-steel holder as well as brass thermal link are constant and equal to environmental temperature T_e. The heat released in ring zones propagates through the copper cavity, brass thermal link and stainless-steel holder. The internal surface of a cavity looses the heat due to radiative heat transfer through the cavity aperture. We have supposed that there are no conductive heat losses through the thermal insulation.

4.2. Radiation Losses from Cavity Internal Surface

Let us assume that there is no heat exchange among points placed on a cavity internal surface due to its very small temperature non-uniformity. Heat flux density that leaves a point on a cavity internal surface at temperature T and escapes through the edge cut of a stainless-steel hood directly or after one or more reflections is equal

$$q = \varepsilon\sigma\left(T^4 - T_e^4\right)F\,, \tag{6}$$

where ε is the total hemispherical emissivity, $\sigma = 5.6704\times10^{-8}$ W m^{-2} K^{-4} is Stefan-Boltzmann constant, T_e is environmental temperature, F is the resolving view factor between that point and hood's edge cut.

Resolving view factor between surfaces A_1 and A_2 defines as a ratio of radiant power, emitted by A_1 to radiant power falling onto A_2 directly and after every possible reflection from A_1 and all intermediate surfaces [29].

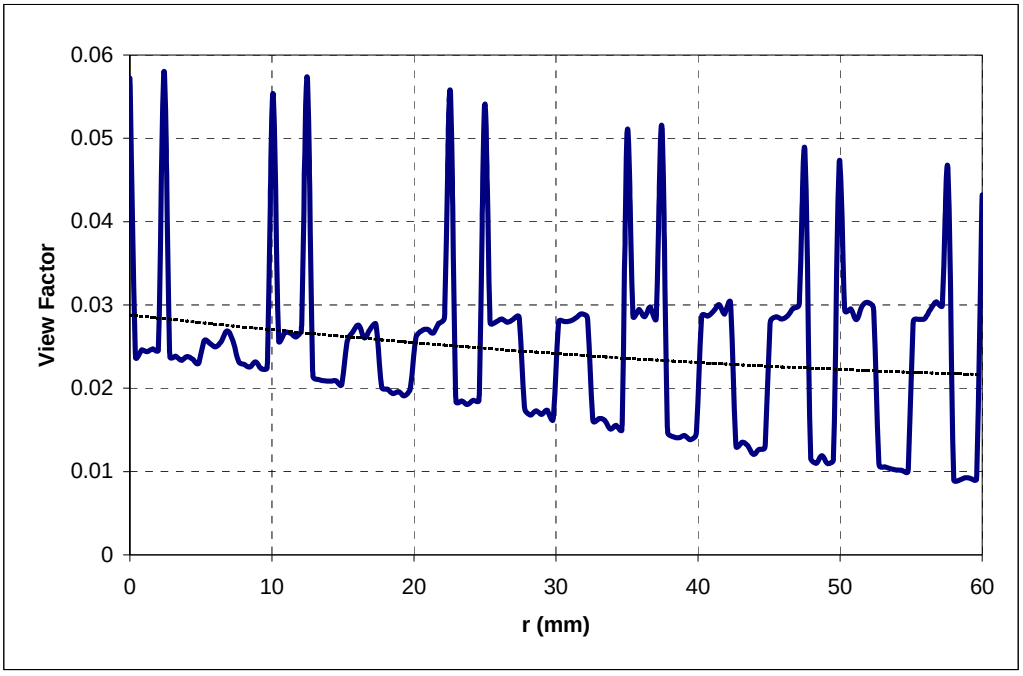

Fig. 6. Distribution of resolving view factors along the radius of cavity bottom.

In order to compute the resolving view factors from a point on internal cavity wall to the edge cut of stainless-steel hood, we used the customized version 4V of STEEP3 program. The algorithm employed is based on the calculation of statistical weights of rays, emitted by the given point on cavity generatrix and escaped through the hood's opening.

The computed distribution of resolving view factors along the radius of a cavity bottom is presented in Fig. 6. The peaks belong to flat areas in the peaks and valleys of concentric grooves, lower plateaus – to internal and external sidehills. The dashed line depicts the trend obtained by the moving average method. The distribution of resolving view factors along cavity lateral walls and brass tube is shown in Fig. 7. The distributions presented in Fig. 6 and Fig. 7 were used for finite-element modeling of steady-state temperature distribution along cavity internal surface.

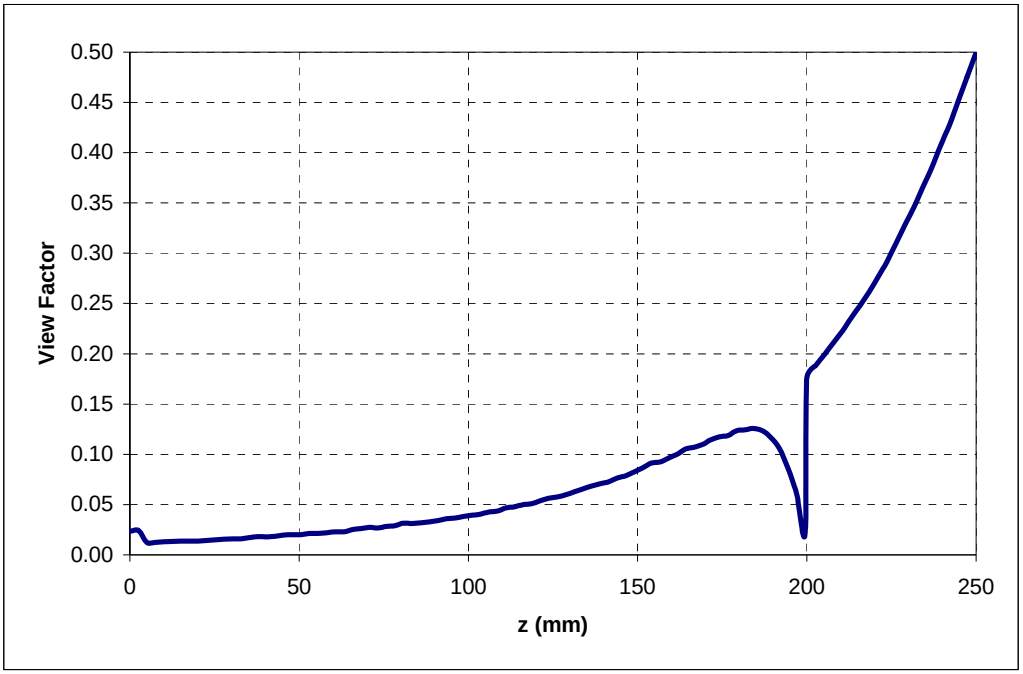

Fig. 7. Distribution of resolving view factors along cavity lateral walls and brass tube (thermal link).

4.3. Thermophysical Modeling using ANSYS 8.0

We used finite-element program ANSYS 8.0 [30] and thermophysical model depicted in Fig. 5 together with the following parameters:

- Thickness of bottom – 15 mm

- Thickness of cylindrical walls and diaphragm – 12 mm
- Stainless-steel holder thickness – 1 mm
- Brass heat link thickness – 1 mm
- Total thickness of black coating and ground – 0.1 mm

We used the following values k of thermal conductivity for materials employed:

- Copper, k_{Cu} = 393 W/(m K)
- Brass, k_{Br} = 130 W/(m K)
- Stainless steel, k_{SS} = 15 W/(m K)
- Black coating and ground, k_b = 1 W/(m K)

At the first stage we supposed that the bottom has no grooves. For modeling, we employed the multi-layer shell finite elements of triangular shape. Due to axial symmetry of a blackbody, we studied only its 30º sector (Fig. 8). The resulting finite element model is shown in Fig. 9.

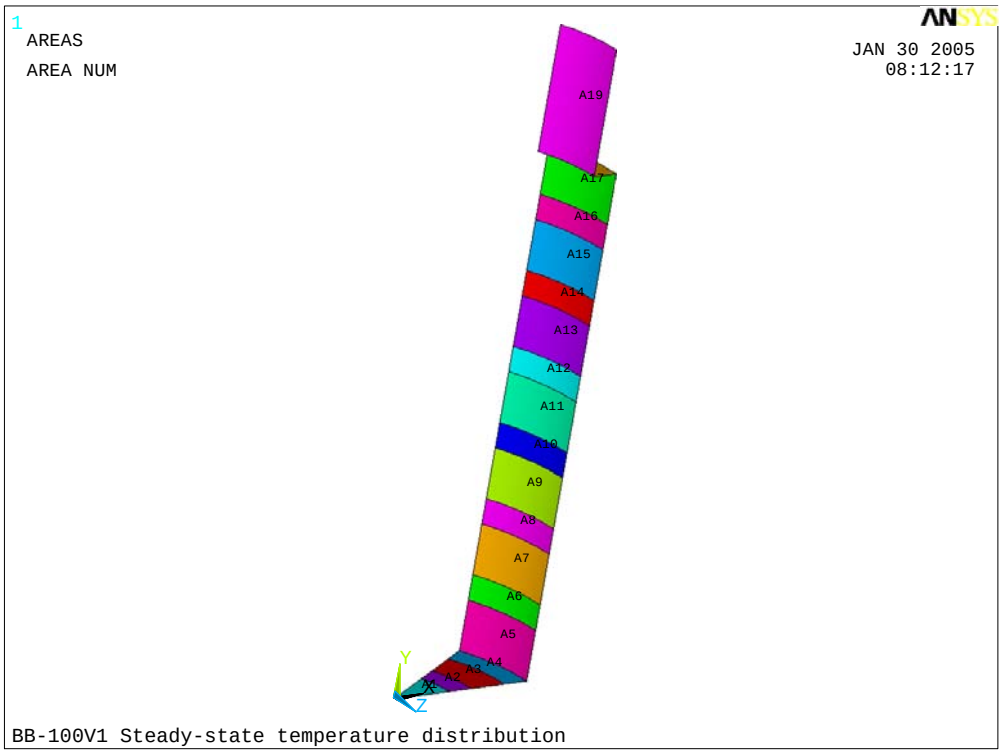

Fig. 8. The sectorial shell model of BB100-V1: even numbers of areas (A2 to A16) correspond to coils of tube with a liquid agent.

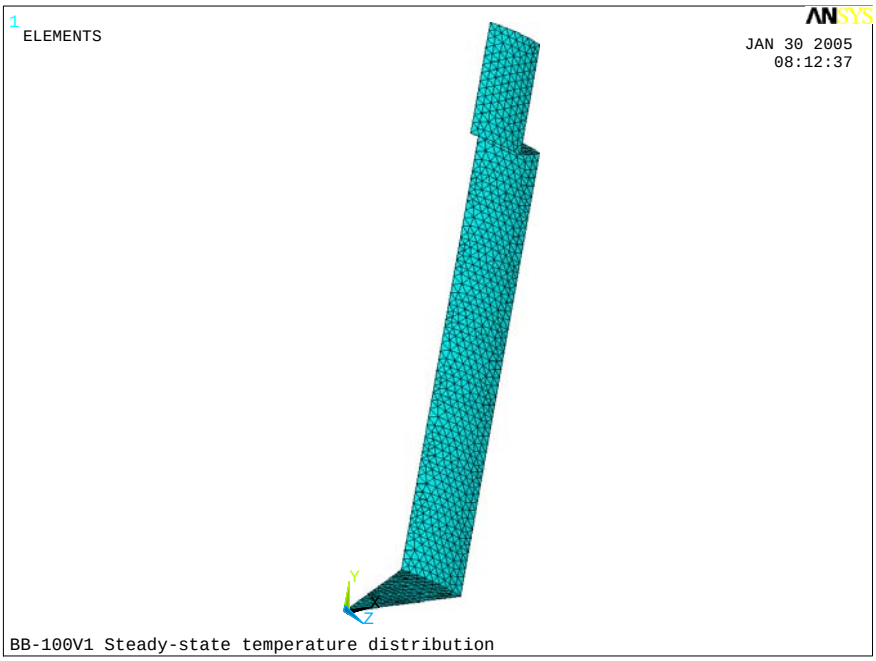

Fig. 9. The finite element model of BB100-V1.

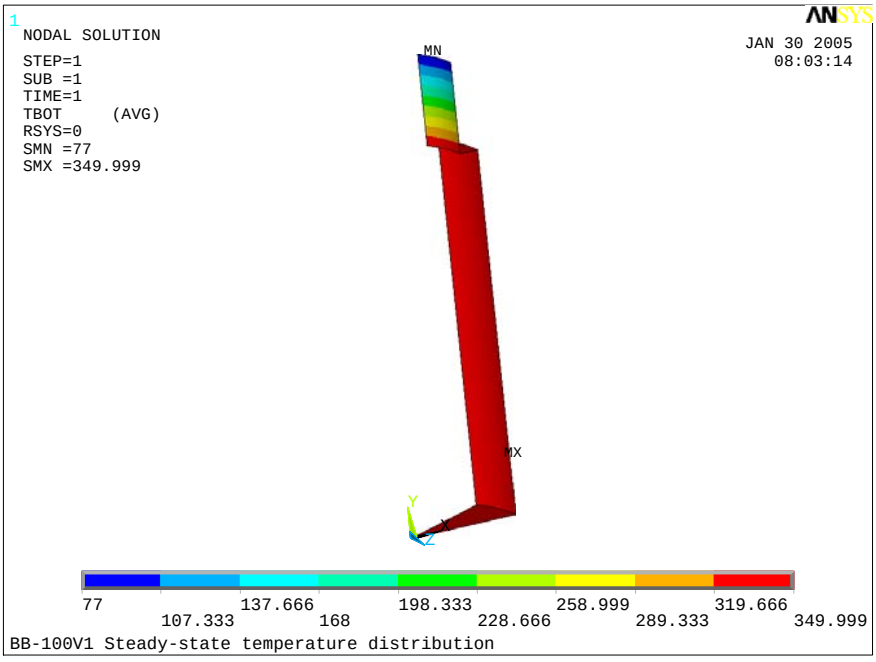

Fig. 10. Steady-state temperature distribution over cavity internal walls.

The computed steady-state temperature distribution over internal cavity walls is depicted in Fig. 10, 11, 12, and 13. Temperature of a liquid agent is 350 K, temperature of environment is 77 K. Obviously, this is a “worst” case, when the temperature non-uniformity is greatest.

Finally, we built the solid finite-element model of a “tooth” – selected annular area of a grooved bottom. Because the radial temperature gradient along the bottom is negligible (about 4 mK, as one can see in Fig. 13), we considered adiabatic the vertical cylindrical surfaces in Fig. 14. On the flat and inclined surfaces of a “tooth”, the radiative heat losses were determined according to Fig. 6 and Eq. 6. Computed temperature drop (see Fig. 15) does not exceed 4 mK. The average temperature of grooved surface differs from temperature of liquid agent on approximately 15 mK.

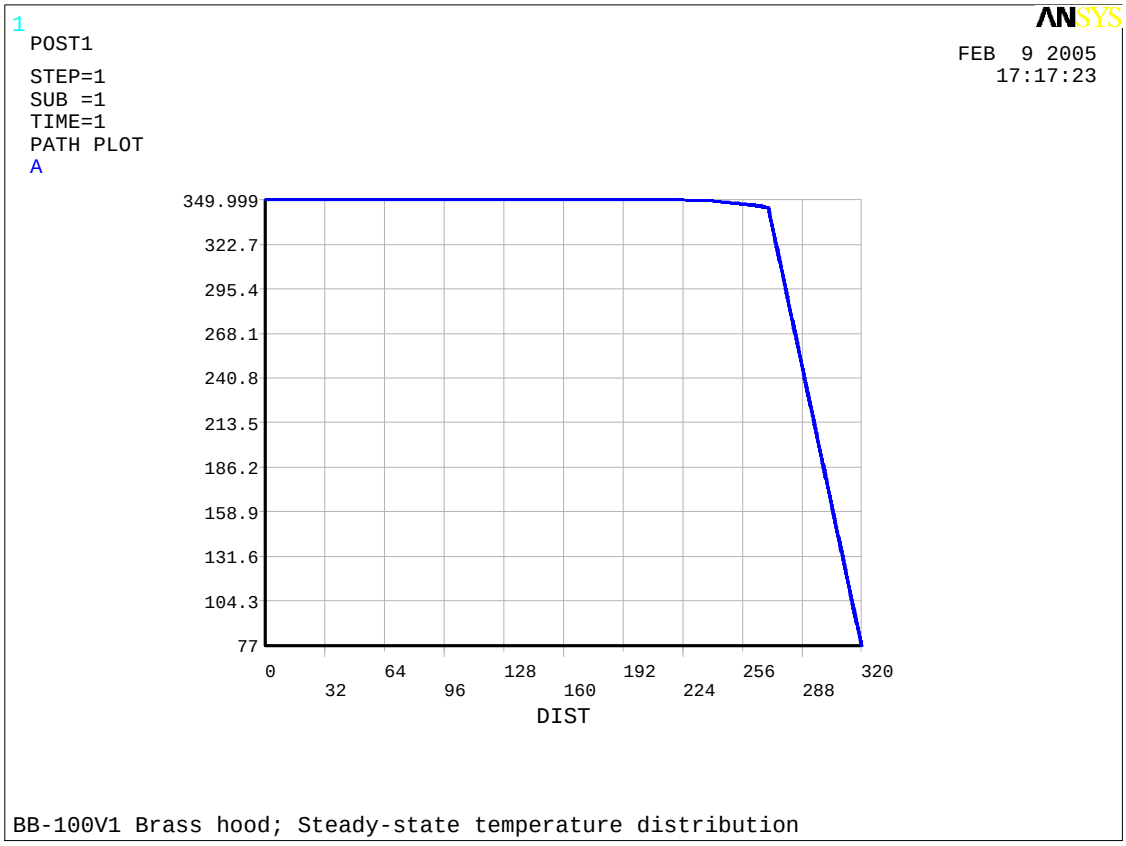

Fig. 11. Temperature distribution along cavity internal generatrix and brass tube.

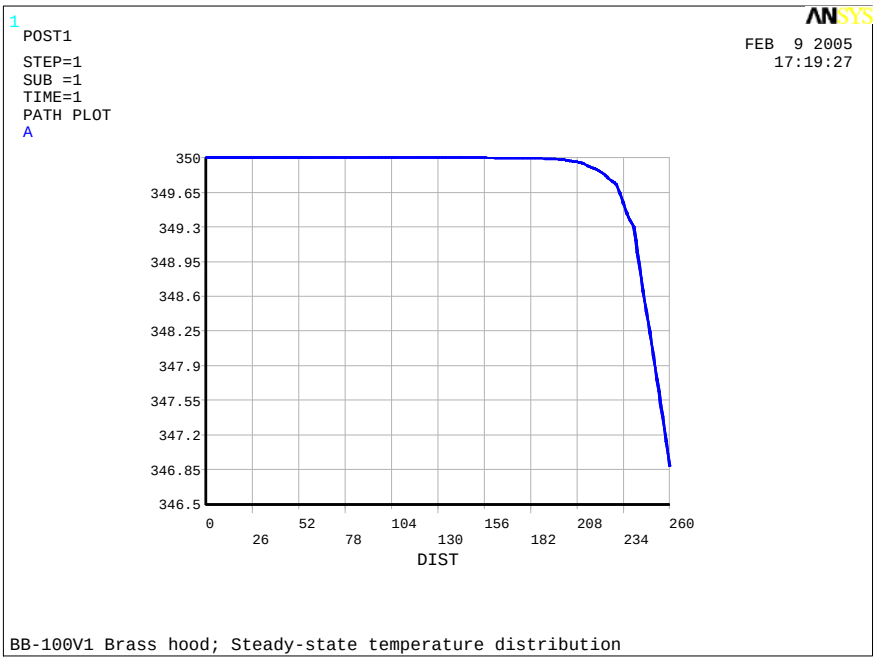

Fig. 12. Steady-state temperature distribution along cavity bottom (0<DIST<60 mm) and cylindrical wall (60<DIST<260).

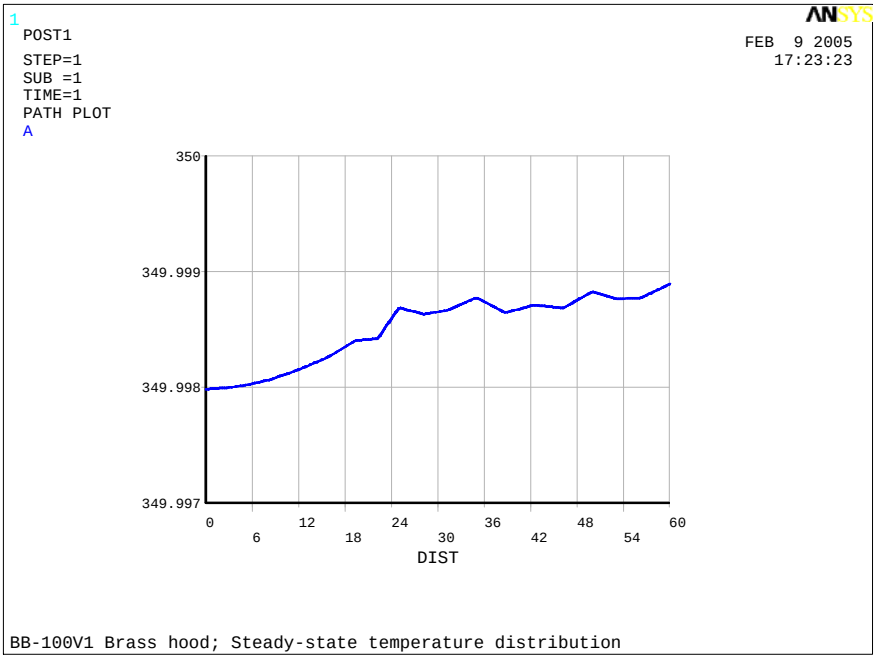

Fig. 13. Steady-state temperature distribution along cavity bottom (0<DIST<60 mm).

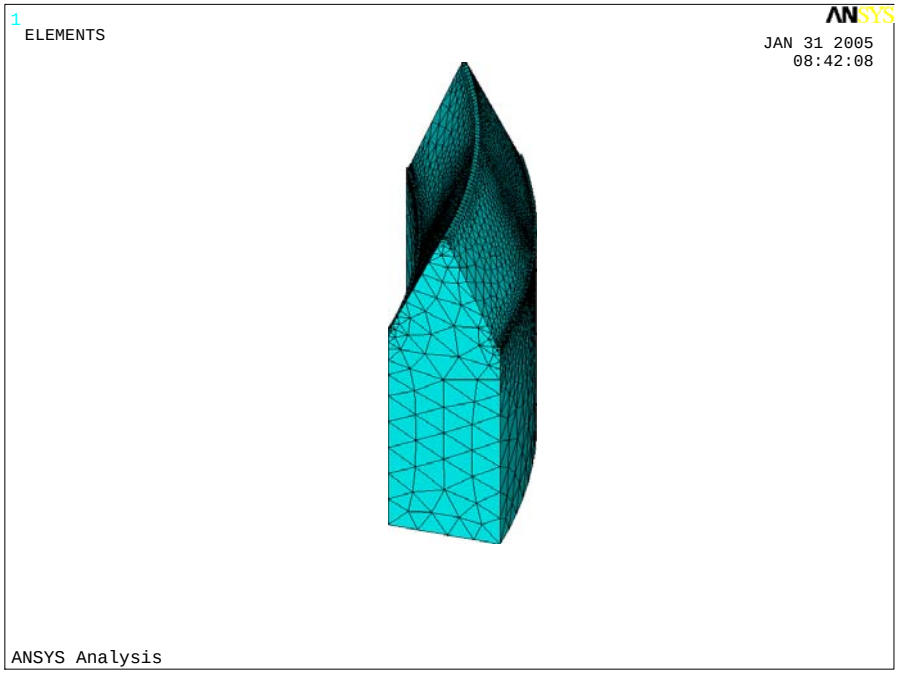

Fig. 14. Solid finite-element model of a “tooth”.

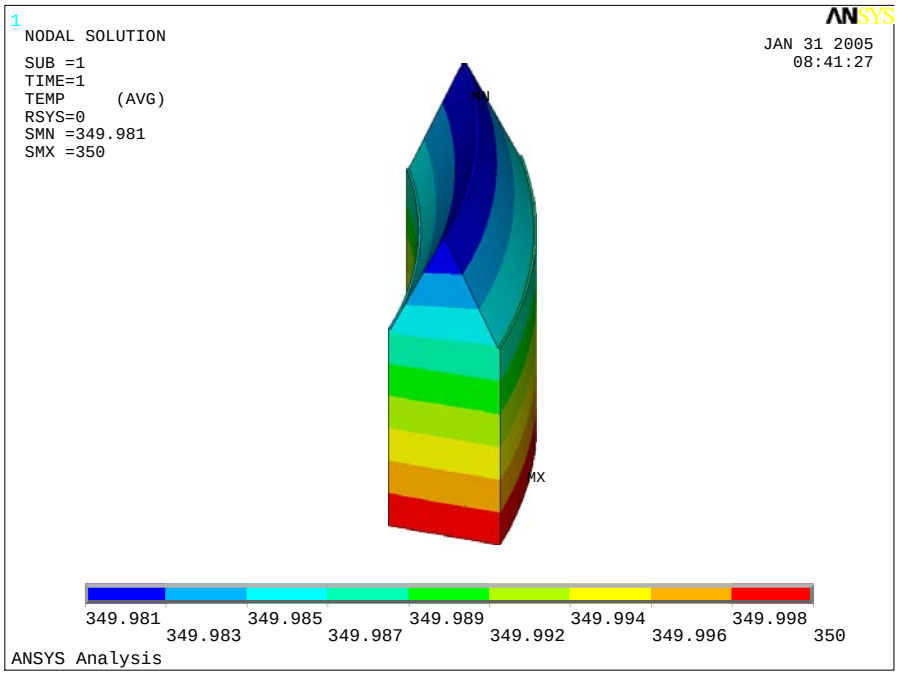

Fig. 15. Steady-state temperature distribution across the “tooth” on the cavity bottom.

5. Evaluation of Thermal Inertia Constant

At the current stage of design, we can perform only crude estimation of blackbody thermal inertia constant (time constant) using the lumped equivalent electric chain depicted in Fig. 16.

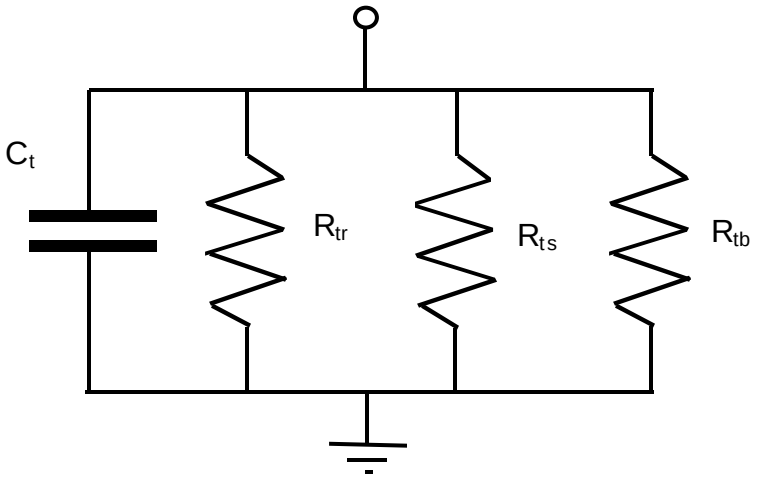

Fig. 16. Equivalent thermal-electric scheme for calculation of time constant.

We will define the thermal resistance as

$$R_t = \frac{\Delta T}{Q} \quad \left[\frac{K}{W}\right], \tag{7}$$

where ΔT is a difference of temperatures, Q is a heat flux.

If C_t is the total heat capacity of a blackbody; R_{ts} and R_{tb} are the thermal resistances due to conductive heat losses through the stainless-steel and brass tubes, respectively; R_{tr} is the thermal resistance due to radiative heat losses, then the time constant is determined by expression

$$\tau = \frac{C_t}{\frac{1}{R_{tr}} + \frac{1}{R_{ts}} + \frac{1}{R_{tb}}}. \tag{8}$$

Thermal resistance due to conductive heat losses through the stainless-steel tube is equal

$$R_{ts,b} = \frac{h}{2\pi R_h d_h k_{s,b}}, \tag{9}$$

where h = 0.05 m, R_h = 0.050 m and 0.051 m, and d_h = 0.001 m are length, radius, and thickness of both brass and stainless-steel tube, respectively.

Mean thermal resistance due to radiative heat losses is equal

$$R_{tr} = \frac{T - T_e}{\varepsilon\sigma\left(T^4 - T_e^4\right)A\overline{F}}, \tag{10}$$

where A = 0.0867 m^2 is the total area of cavity internal surface, $\overline{F} \approx 0.04$ is the mean value of resolving view factor on this surface.

The specific heat capacity of copper at 350 K is 392.6 J/(kg K), density is 8920 kg/m^3, the volume of copper cavity is about 1.341×10^{-3} m^3. Then the cavity mass is about12 kg, and C_t = 4716 J/K.

The computation by the Eq. 8 – 10 gives the value of τ = 82.5 min.

Thermal inertia constant τ is the quantity that describes the reaction of a blackbody on the step change of the temperature of its bound. So, let we have a blackbody with temperature T_1 and the liquid agent pre-heated up to temperature $T_0 > T_1$ for $t < 0$. Let we need to heat up the blackbody up to 350 K. If at the moment of time t = 0 liquid begins to flow from thermostat through the coils wrapped around the blackbody, the blackbody mean temperature T will change according to equation

$$T(t) = T_1 + (T_0 - T_1)\left(1 - e^{-\frac{t}{\tau}}\right). \tag{11}$$

When t = τ, the change of temperature will be about $0.632\times(T_0 - T_1)$. After 5τ, the change of temperature of a blackbody will be about $0.99\times(T_0 - T_1)$. When $T_0 < T_1$, the following equation for cooling is in use:

$$T(t) = T_0 - (T_0 - T_1)e^{-\frac{t}{\tau}}. \tag{12}$$

For example, for T_1 = 77 K, T_0 = 350 K, at $t = \tau$, the temperature of blackbody will be about 249 K. However, if we set T_0 = 500 K, the temperature of blackbody at $t = \tau$ will be about 344 K.

Real thermostatic systems use these relationships and employ the sophisticated algorithms to change the liquid agent temperature and minimize the transition time that can be significantly less than the thermal inertia constant τ.

6. Monte Carlo Modeling of BB-100V1 Effective Emissivity

We have computed the normal spectral effective emissivities for two limiting values of cavity wall emissivity (0.935 and 0.990) and two temperature distributions obtained by the FEA for two values of thermostating liquid (350 K and 240 K). The environmental temperature in all cases is 77 K; diffusity of cavity walls is 0.7.

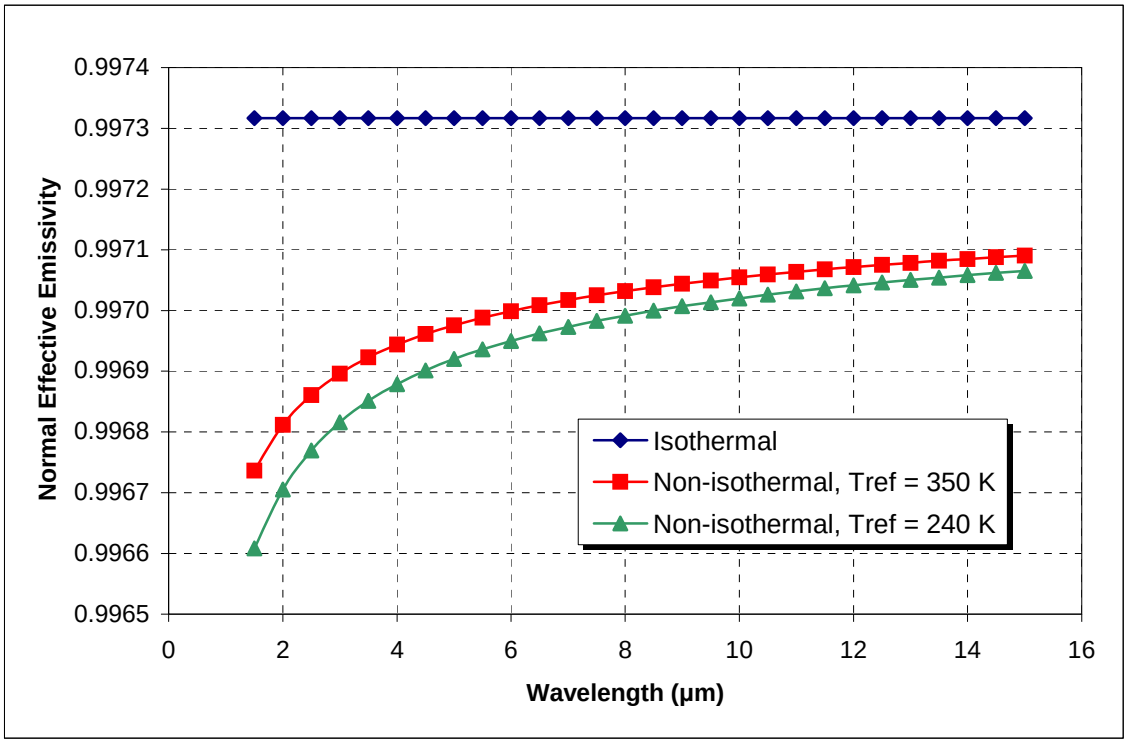

Fig. 17. Normal spectral effective emissivity of BB100-V1 for 3 temperatures distributions; wall emissivity is 0.935

The results of computations are depicted in Fig. 17 and Fig. 18. The data analysis and numerical experiment additionally performed shown that these values of effective emissivity do not change significantly for oblique viewing up to angles of ±4.5º with cavity axis. No background radiation effects were detected.

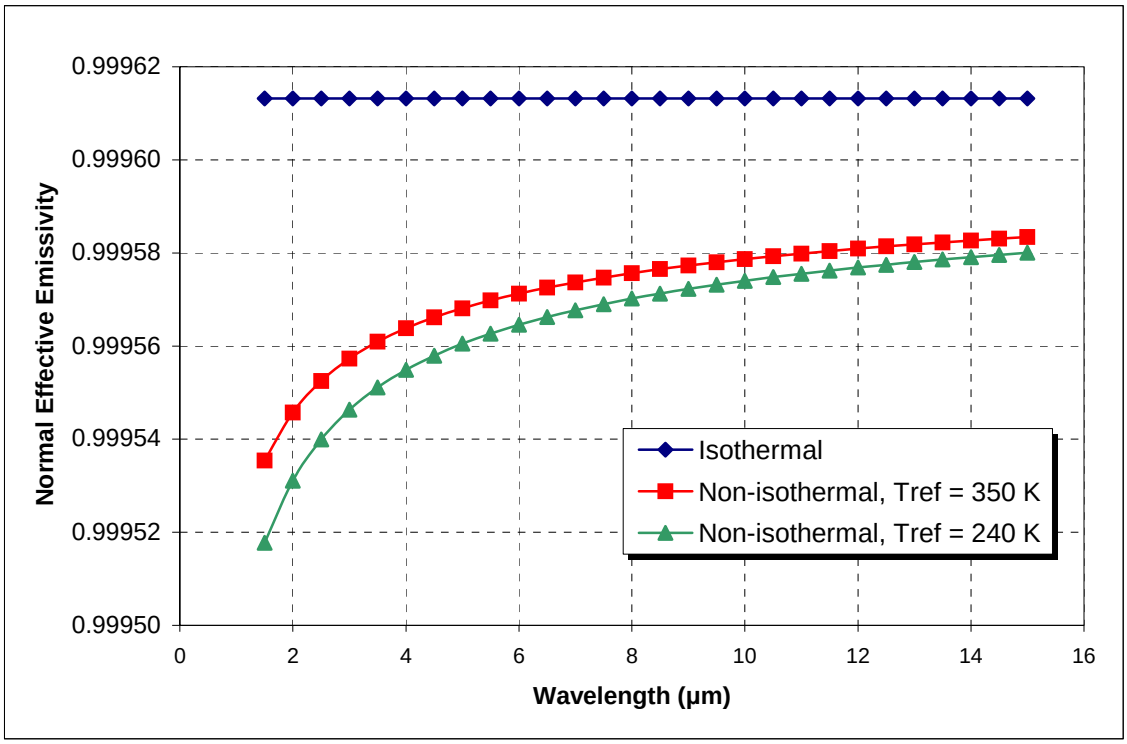

Fig. 17. Normal spectral effective emissivity of BB100-V1 for 3 temperatures distributions; wall emissivity is 0.990

7. BB-100V1 Preliminary Design

The drawing of BB100-V1 preliminary design performed with the account of above-mentioned studies is depicted in Fig. 18.

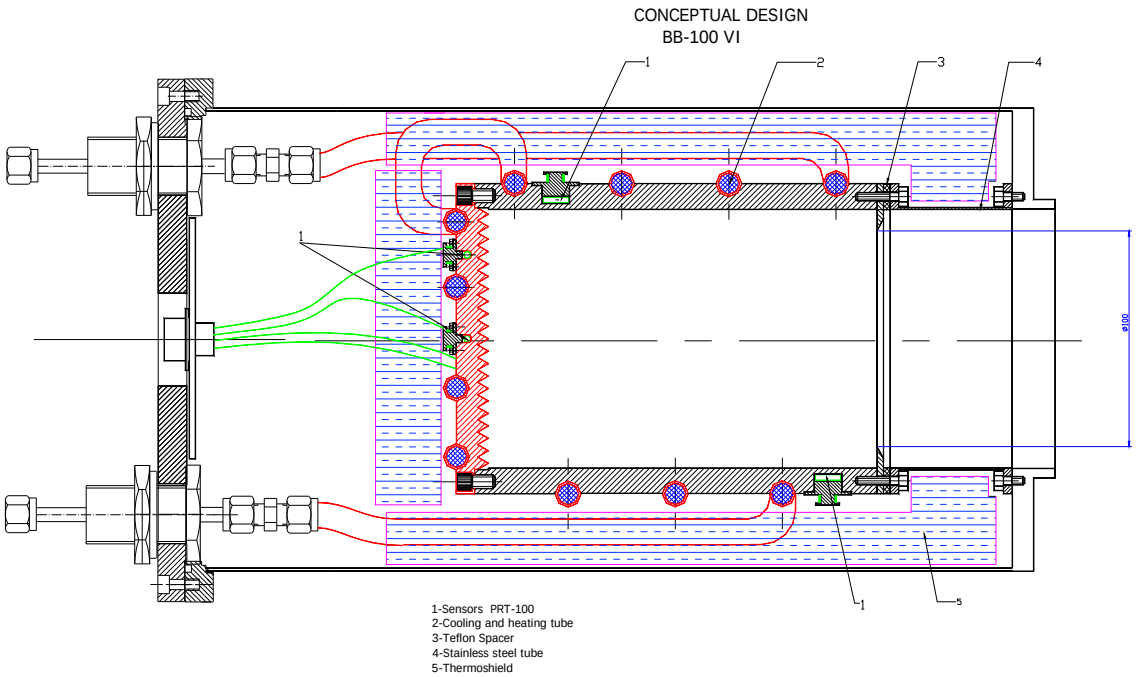

Fig. 18. BB100-V1 preliminary design.

8. References

1. S. M. Pompea and R. P. Breault, "Black surfaces for optical systems". Handbook of Optics, Vol. 2, pp. 37.1-37.63, Ed. by M. Bass, (McGraw-Hill, New York, 1995)
2. Persky M J 1999 Review of black surfaces for space-borne infrared systems *Rev. Sci. Instr.* **70** 2193-2217
3. Meier S R 2001 Characterization of Highly Absorbing Black Appliqués in the Infrared *Appl. Opt.* **40** 2788-2795
4. Betts D B, Clarke F J J, Cox L J, Larkin J A 1985 Infrared Reflection Properties of Five Types of Black Coating for Radiometric Detectors *J. Phys. E: Sci. Instrum.* **18** 689-696
5. Willey R R, George R W, Ohmart J G, Walvoord J W 1983 Total Reflectance Properties of Certain Black Coatings (From 0.2 to 20.0 micrometers) *Proc. SPIE* **384** 19-26
6. De Silva A A, Jones B W 1987 Bidirectional Spectral Reflectance and Directional-hemispherical spectral reflectance of six Material used as Absorbers of Solar Energy *Solar Energy Materials* **15** 391-401
7. Envall J, Kärhä P, Ikonen E 2004 Measurements of Fibre Optic Power Using Photodiodes with and without an Integrating Sphere *Metrologia* **41** 353-358
8. Kwor E T, Matteï S 2001 Emissivity Measurements for Nextel Velvet Coating 811-21 between –36ºC and 82ºC *High Temp.-High Pressure* **33** 551-556
9. Wood B E, Pipes J G, Smith A M, Roux J A 1976 Hemi-ellipsoidal Mirror Infrared Reflectometer: Development and Operation *Appl. Opt.* **15** 940-950
10. Batuello M, Clausen S, Hameury J, Bloembergen P 1999 The Spectral Emissivity of Surface Layers, Currently Applied in Blackbody Radiators, Covering the Spectral Range from 0.9 to 20 µm. An International Comparison *TEMPMEKO '99 Proceeding* 601-606
11. Lohrengel J, Todtenhaupt R 1996 Wärmeleiftfähigkeit, Gesamtemissionsgrade undspktrle Emissionsgrade der Beschichtung Nextel-Velvet-Coating 811-21 (RAL 900 15 tiefschwarz matt) *PTB-Mitteilungen* **106** 259-265
12. Hameury J, Hay B, Filtz J R 2003 Measurement of Infrared Spectral Directional Hemispherical Reflectance and Emissivity at BNM-LNE – Paper presented at the Fifteen Symposium on Thermopysical Properties, June 22-27, 2003, Boulder, CO, USA
13. Mankiewicz Gebr. & Co., Georg-Wilhelm-Straße 189, D-21107 Hamburg, Telefon: + 49 (0) 40 75 10 30; Telefax: + 49 (0) 40 75 10 34 15; E-Mail: info@mankiewicz.de or Mankiewicz-Coatings LLC, 8 Carlisle Drive, Simpsonville, South Carolina 29681, USA; Tel.: +1 - 86 49 62 66 90, Fax: +1 - 86 49 62 67 40, E-Mail: sales@mankiewicz-coatings.com, tech.info@mankiewicz-coatings.com
14. Chu B, Machin G 1999 A Low-temperature Blackbody Reference Source to -40º C *Meas. Sci. Technol.* **10** 1-6

15. Hartmann J, Fisher J 1999 Radiator standards for accurate IR calibrations in remote sensing based on heatpipe blackbodies *Proc. SPIE* **3821** 395-403
16. Mester U, Winter P 2001 New Blackbody Calibration Source for Low Temperatures from –20 to +350 ºC *Proc. SPIE* **4360** 372-379
17. Chu B, McEvoy H C, Andrews J W 1994 The NPL Reference Sources of Blackbody Radiation *Meas. Sci. Technol.* **5** 12-19
18. Fowler J B 1995 A Third Generation Water Bath Based Blackbody Source *J. Res. Natl. Inst. Stand. Technol.* **100** 591-599
19. Fowler J B 1996 An Oil-Bath-Based 293 K to 473 K Blackbody Source *J. Res. Natl. Inst. Stand. Technol.* **101** 629-637
20. Té Y, Jesek P, Camy-Peyret C, Payan S, Briaudeau S, Fanjeaux M 2003 High Emissiviy Blackbody for Radiometric Calibration Near Ambient Temperature *Metrologia* **40** 24-30
21. Té Y, Jesek P, Camy-Peyret C, Payan S, Perron G, Aubertin G 2002 Balloonborne Calibrated Spectroradiometer for Atmospheric Nadir Sounding *Appl. Opt.* **41** 6431-6441
22. Morozova S P, Morozov P A 2002 High Precision Blackbody Sources and Facilities developed at VNIIOFI, Russia *Proc. SPIE* **4710** 1-8
23. Sapritsky V I, Ogarev S A, Khlevnoy B B, Samoylov M L, Khromchenko V B, Morozova S P 2002 Dissemination of ultra-precise measurements in radiometry and remote sensing within 100…3500 K temperature range on the base of blackbody sources developed in VNIIOFI *Proc. SPIE* **4818** 127-136
24. STEEP3, version 1.3. User's Guide. Virial, Inc., NY, 2000
25. Sapritsky V I and Prokhorov A V Calculation of the Effective Emissivities of Specular-Diffuse Cavities by the Monte Carlo Method 1992 *Metrologia* **29** 9-14
26. Sapritsky V I and Prokhorov A V 1995 Spectral effective emissivities of nonisothermal cavities calculated by the Monte Carlo method *Appl. Opt.* **34** 5645-5652
27. Prokhorov A V, Mekhontsev S N, Hanssen L M 2003/2004 Emissivity modeling of thermal radiation sources with concentric grooves *High Temp. - High Press.* **35/36** 199-207
28. Murthy A V, Prokhorov A V, DeWitt D P 2004 High Heat-Flux Sensor Calibration: A Monte Carlo Modeling *J. of Thermophysics and Heat Transfer* **18** 333-341
29. Siegel R D, Howell J R 1992 Thermal Radiation Heat Transfer, 3rd ed., Hemisphere Publishing, Washington, DC
30. Moaveni S 2003 Finite Element Analysis: Theory and Applications with ANSYS, 2nd Ed. Prentice Hall, Upper Saddle River, NJ